SUBCONTRACT TITLE: Innovative Characterization of Amorphous and Thin-Film Silicon for Improved Module Performance

SUBCONTRACT NO: NREL Subcontract ZXL-5-44205-11

QUARTERLY TECHNICAL STATUS REPORT: Phase III/Quarter 2
28 July 2007 to 15 November 2007

SUBMITTED TO: Bolko von Roedern
National Renewable Energy Laboratory

PRINCIPAL INVESTIGATOR: J. David Cohen, Department of Physics
University of Oregon, Eugene, OR 97403

This report covers the second quarter of Phase III for the period 28 July 2007 to 15 November 2007 of the Thin Film Partnership Subcontract ZXL-5-44205-11. Our Statement of Work calls for us to devote roughly 30% of our effort to CIS thin-film photovoltaics, and 70% to silicon-based thin film technologies. Accordingly, this Quarterly will be devoted to reporting the some of our results obtained studying CIGS cells. The primary results to be reported from work in my laboratory during this period concerns the continuation of our studies to try to better understand the effects of Na impurities on CIGS device performance. In particular, we extended our studies by carrying out a more detailed analysis of the differences in deep defect distributions for the samples with and without normal levels of Na. We also began examining in the differences in the light-induced metastable changes and annealing kinetics for CIGS samples with normal and reduced levels of sodium.

It is well known that fabricating $Cu(In_xGa_{1-x})Se_2$ (CIGS) thin-film photovoltaic devices on glass substrates containing sodium can boost the efficiency of the device by up to 50 %. Nonetheless, there is a surprising lack of consensus on how Na affects the CIGS network at the atomic level. For example, some published results claim that Na only acts during the growth of the CIGS[1], while others have found similar benefits to adding Na in a post-deposition treatment[2]. Similarly, there is disagreement as to whether the Na acts in the bulk of the absorber[3] or only at the grain boundaries[4]. Researchers have also tried to understand the role of Na by investigating its effect on both the Se incorporation and the Ga content in the samples.[5]

All samples used in this study were fabricated at the Institute of Energy Conversion at the University of Delaware. Two pairs of co-deposited samples were examined. In each case one sample utilized the usual soda-lime glass substrate while the companion sample was deposited simultaneously on a substrate which substantially eliminated sodium from the resultant CIGS film. In all cases, Mo was deposited onto the substrates, followed by layers of CIGS/CdS/ZnO/ITO/Ni-Al grids deposited in the standard manner.[6] The first set examined (A) and reported upon last year compared a device fabricated directly on soda lime glass to a device fabricated on a SiO_2 diffusion barrier over the soda lime glass to inhibit the incorporation of Na. SIMS profiling later revealed that the diffusion barrier only cut the Na concentration by 1-2 orders of magnitude, depending on profile depth (with more Na close to the diffusion barrier).[7] In May 2007 a second pair of matched samples (B) was prepared, comparing a device deposited onto a Ti substrate with one deposited on standard soda lime glass. The

Table 1: Device performance parameters of the matched CIGS devices with and with less Na.

Deposition	Sample	V_{OC} (V)	J_{SC} (mA/cm^2)	FF (%)	Eff (%)
A	CIGS on Soda-lime Glass	0.624	32.9	74.0	15.2
	Reduced Na CIGS (SiO_2 barrier)	0.494	33.6	64.3	10.7
B	CIGS on Soda-lime Glass	0.651	29.9	77.1	15.0
	Na free CIGS (Ti substrate)	0.522	30.1	65.1	10.2

substrate temperature during deposition for all samples was 550 °C, and each contained a CIGS absorber roughly 2.0μm thick. Ultimately, we found no substantial differences between the properties of the sample deposited on the SiO_2 coated glass substrate or the sample deposited on the Ti substrate. Table 1 provides typical performance parameters for the cells studied, and illustrates the well known effects of Na on CIGS devices; namely, a ~130meV increase in V_{OC}, leading to a nearly 50 % increase in efficiency, with little effect on the short circuit current.

A variety of our junction capacitance measurements were used to examine the sub band-gap defect properties of the samples. Admittance spectroscopy was used to probe the electrical response of the sample over a range of frequencies and temperatures. Drive level capacitance profiling was used to determine the free carrier density and defect density of the samples, as has been described in detail elsewhere.[8] Sub-band-gap optical absorption-like spectra were obtained from the transient photocapacitance (TPC) method on the samples from deposition A and reported last year. Those TPC spectra revealed that the Urbach energy (which becomes larger with increasing structural and compositional disorder) was somewhat larger (23meV *vs.* 17meV) in the sample without Na and that the defect bands were of similar magnitudes but had a somewhat different energy distribution. However, such differences seemed likely to account for the very different performance parameters indicated in Table 1.

Drive-level capacitance profiles for a range of measurement temperatures are displayed in

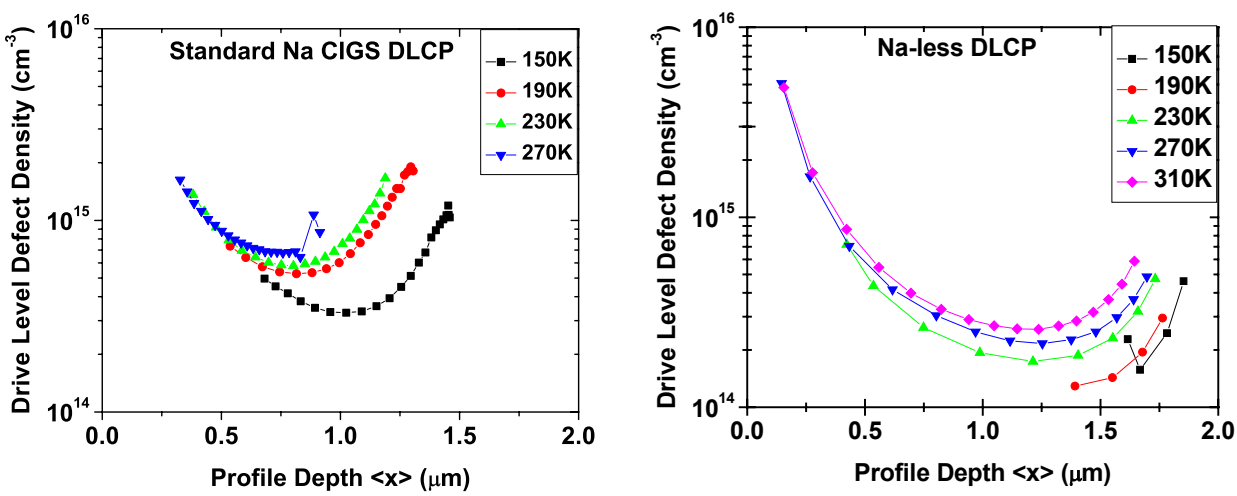

FIG. 1. (a) Spatial defect profiles from DLCP for the standard Na sample and (b) for the sample without Na. These profiles were obtained at 10 kHz at the temperatures indicated with an applied dc bias ranging from at least 1.0 V reverse to 0.3 V forward. For the standard sample the profiles indicate a hole carrier densities in the mid 10^{14} cm^{-3} range and a similar deep acceptor density. For the sample without Na they indicate a free hole carrier density near 2 x 10^{14} cm^{-3} and very low deep acceptor density of roughly 1 x 10^{14} cm^{-3}.

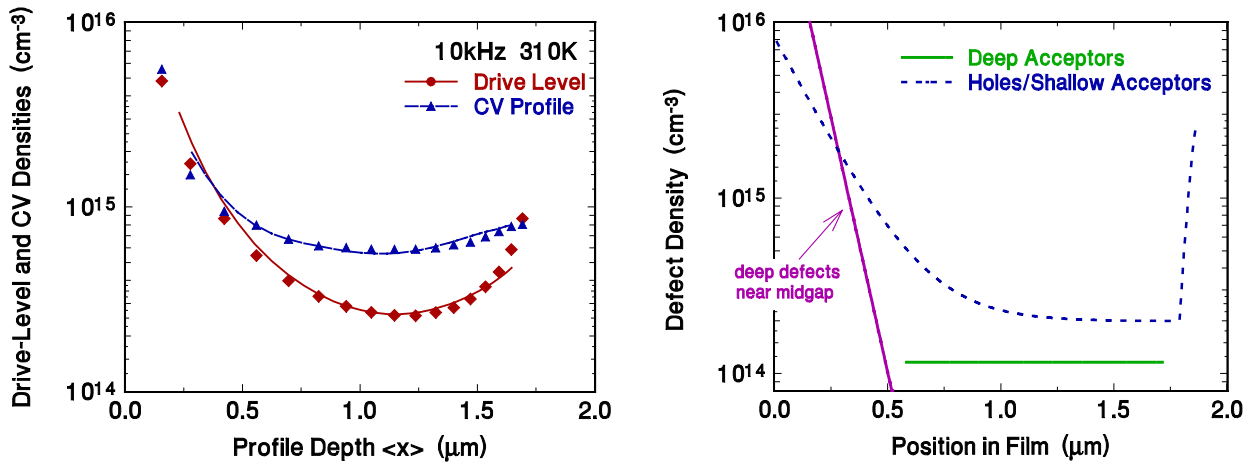

FIG. 2. (a) Simulated fits are shown (solid lines) to the DLCP and CV profiles (symbols) at 310K. **(b)** Defect distributions used to simulate the data in 2(a). To account for the large difference between the two types of profiles, we deduced the presence of a large exponentially varying distribution of mid-gap deep defects was located near the barrier interface as shown. The fits also incorporated a low (~10^{14} cm^{-3}) density of bulk deep of acceptors near E_V + 0.35eV indicated by the horizontal dashed line; however, its affect on the profiles was too low to deduce an accurate spatial profile. The distribution of holes/shallow acceptors is shown by the dashed line. Its rapid rise near 1.8 µm was used to simulate the effect of the back conducting contact.

Fig. 1 for the CIGS samples from deposition B, with and without Na, in their annealed states. These profiles show similar overall shapes but indicate a somewhat higher density and spatial variation in the standard sample with Na. That sample also shows a deep acceptor activating between 190 K and 230 K that is largely absent in the sample without Na. Instead, those profiles indicate a low hole carrier density (near 2 x 10^{14} cm^{-3}) and very low deep acceptor density (roughly 1 x 10^{14} cm^{-3}). Given this low defect density compared to the companion standard sample (with a deep acceptor density roughly an order of magnitude higher), it initially seemed surprising that its performance was substantially poorer. This indicated that something not visible in the DLC profiles must be causing the reduction in performance of cell without Na.

A comparison of the DLCP and CV profiles for the sample without Na shown in Fig. 2(a) provides a likely explanation. Because the CV profile is so much higher than the highest temperature DLCP profile, this indicates that the difference cannot simply be attributed to deep defects in the bulk region of the CIGS absorber. (In contrast, the DLCP and CV profiles are nearly identical in many cases at higher temperatures for CIGS samples with standard levels of Na.)

To be able to accurately interpret the types of results shown in Fig. 2(a) we recently extended our computer modeling capabilities to include the effects from both the usual deep acceptors and also from a much deeper band of midgap defects. We also added the ability to examine a wider range of possible spatial variations. The details of these improvements in computer modeling will be reported later. The deduced defect distributions are shown in Fig. 2(b) and these resulted in the very good fits to the profiling data shown by the solid lines in Fig. 2(a). These fits indicate that the substantially larger CV profile value actually arises from a large concentration of defects (roughly 10^{17} cm^{-3}) located within about 700Å of the barrier interface.

Such a large defect density in close proximity to the CdS/CIGS interface could easily result in the 130mV observed reduction in V_{OC} compared to the samples with normal Na levels.

Indeed, by integrating Poisson's equation we can estimate the loss in V_{OC} due to charged defects in the vicinity of the barrier interface; specifically,

$$\Delta V_{OC} = \frac{1}{\varepsilon}\int_0^\infty x\rho(x)dx \approx \frac{qN_{\text{int}}d}{\varepsilon} \quad , \tag{1}$$

where qN_{int} is the total sheet charge density present near the open circuit voltage condition, and d is the width of its spatial distribution from the barrier interface. The inferred defect distribution from the fits in Fig. 2 is of just the correct magnitude to account for the observed V_{OC} deficit. Simulated DLCP profiles were also been obtained for the standard (with Na) CIGS profiles of Fig. 1(a). These simulations indicate a significantly larger density of bulk deep defects. They also show some response from defects near the interface; however, that number is lower by nearly two orders of magnitude compared to the sample with reduced Na.

Comparing the admittance spectra for the matched pair of CIGS samples from deposition B with and without Na in figures 3(a) and 3(b) we clearly observe the familiar step-like feature in the former case, indicating a deep acceptor defect level with an activation energy of 270 meV. We also note the lack of such a feature in the capacitance response in the latter case, indicating the absence of a significant density of deep acceptors. This result mirrors the DLCP data of Fig. 1(b) which also indicated a very low deep acceptor responses. We previously reported, however, that a distinct step-like feature does appear, with an activation energy of 360 meV, when admittance is measured under forward bias for the reduced Na sample.[7]

During the past quarter we have been comparing the effects of light-soaking on the

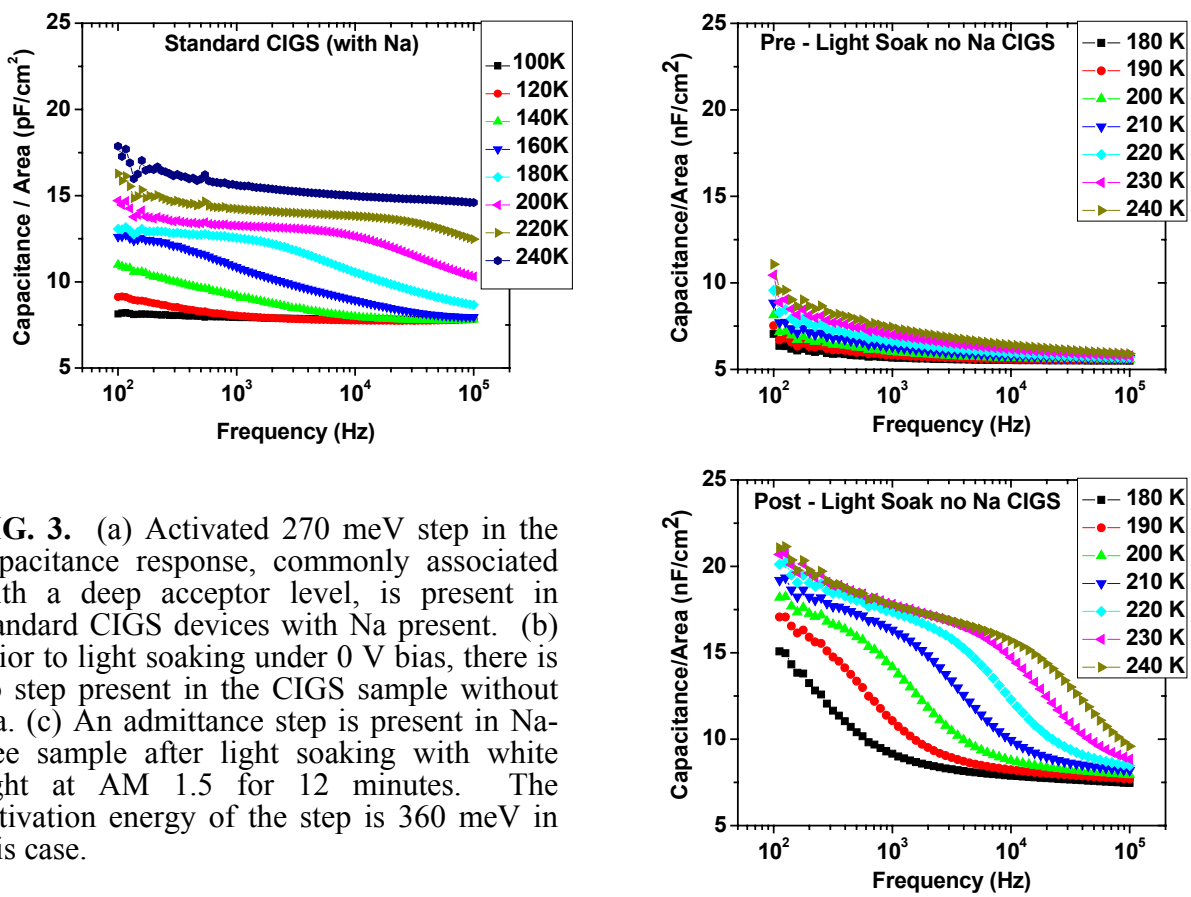

FIG. 3. (a) Activated 270 meV step in the capacitance response, commonly associated with a deep acceptor level, is present in standard CIGS devices with Na present. (b) Prior to light soaking under 0 V bias, there is no step present in the CIGS sample without Na. (c) An admittance step is present in Na-free sample after light soaking with white light at AM 1.5 for 12 minutes. The activation energy of the step is 360 meV in this case.

electronic properties of the CIGS samples with and without Na. One of the most dramatic results is that, after even a few minutes of light soaking with white light, a step in the admittance spectra appears in the sample without Na even under reverse bias, as is illustrated in Fig. 3(c). This step has a nearly activation energy to that which appeared only under forward bias for the fully annealed sample. Moreover, DLCP measurements confirm that the admittance step that appears after light soaking in the sample without Na does indeed correspond to a bulk deep-acceptor like feature.

We then used these DLCP measurements to examine the details of the creation and annealing kinetics of the deep acceptor and hole carrier densities for sample set B, with and without sodium present. The samples were exposed to white light with one sun intensity at 250 K then the temperature was lowered to measure the free carrier and deep defect densities. In the Na-free sample both the free carrier density and deep defect density were measured at 210 K at different frequencies (200 Hz and 80 kHz) positioned above and below the capacitive step to distinguish the two contributions. For the standard CIGS sample the free carrier density was obtained from 80 kHz profiles at 80 K and the deep defect density from 200 Hz profiles at 160K.

Figure 4 summarizes the dramatic difference in creation kinetics between the standard CIGS sample and the sample without Na. The deep acceptor and free carrier densities have been normalized to their annealed state values for both samples. Each series started with exposure to light for 1 second and ended with each sample being light soaked for more than 5 hours (19683s). The sample containing sodium exhibits the nearly 1:1 relationship between the increases in deep acceptor and hole carrier densities as previously reported by Lee, *et al*, under a variety of light soaking and current injection conditions.[9] Equipment limitations required that we measure the free carrier and deep defect densities at different temperatures for this sample, which we believe accounts for the minor deviation from the 1:1 relationship observed in the sample with Na. Thus these data indicate that for every deep (270 meV) acceptor that is created in the sodium sample, there is a corresponding increase in free holes. In stark contrast to this behavior, the sample without sodium shows only a very modest increase in the free carrier density compared to the much larger increase in the deep (360 meV) acceptor density (the rate of increase of ΔN_A compared to Δp exceeds a factor of 3 in this case).

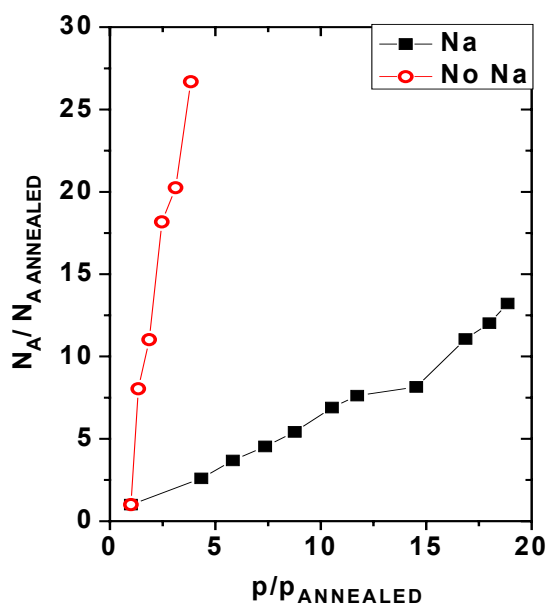

FIG. 4. During light soaking the sample without sodium exhibited a much larger increase in the number of deep acceptors with respect to the increase in the free carrier density than the sample containing sodium. For both cases the deep acceptor density, N_A, and free carrier density, p_A, have been normalized to their values in the annealed state; specifically to N_A= 5.7x10^{13} cm^{-3} and p_A=1.6x10^{14} cm^{-3} for the sample without sodium, and to N_A=7.9x10^{14} cm^{-3} and p_A=3.0x10^{14} cm^{-3} for the sample with sodium.

The annealing kinetics of the light-induced metastable increase in the deep acceptor densities in these two samples were then investigated using an isochronal annealing sequence, with the results shown in Fig. 5. The samples were held at each anneal temperature for 10 minutes, then the temperature was lowered and the free carrier and deep acceptor densities were measured as described above. Although the magnitudes of the densities are different (note the different scales on either side of the graph) the relative annealing behavior is absolutely identical. The identical annealing behavior indicates an identical atomic origin for the metastable behavior in both the standard and Na-free CIGS materials in spite of their different creation kinetics (see discussion below).

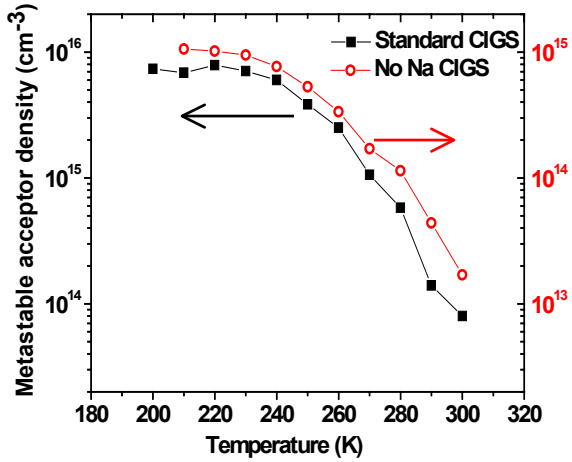

FIG. 5. In spite of the differences in absolute magnitude, and the different relative increases for the free hole densities displayed in Fig. 4, the metastable deep acceptor densities annealed at the exactly the same rate states for both samples.

The behavior of the standard CIGS sample, with a nearly identical increases in deep acceptor and the free carrier densities, is consistent with the light induced transformation of a positively charged gap state defect into a negatively charged gap state. Thus, it supports the model for metastability in CIGS caused by the (V_{Se}-V_{Cu}) complex as proposed by Lany and Zunger.[10] In contrast, for the sample without Na, we observe a clear increase in the shallow acceptor density accompanied by only a very small increase in the free carrier density. Such behavior would be consistent with a shift in gap state energy of some defect complex but without any net change in charge state (for example, a defect whose energy shifts from the upper half of the gap to a position closer to the valence band but still lying above the bulk Fermi energy). This would then result in a very small change in the bulk Fermi level and hence in the density of free hole carriers.

The very different behaviors indicated in the creation kinetics [Fig. 4] might suggest that a very different defect complex must be responsible for the metastable behavior in the 2 types of samples. However, it is generally agreed that the creation kinetics of the light-induced effect depends on the minority carrier concentration which, in turn, depends on the electron recombination rate. Because that recombination rate also depends directly on the hole concentration, which increases very differently in the two types of samples, this could easily account for any differences in *creation kinetics*. In contrast, the *annealing kinetics* for the two types of samples is nearly identical which suggests that the center responsible for the metastable changes must actually be the same for both types of samples.

We are currently considering a number of candidate defect models that might be able to account for the metastable behaviors observed in CIGS with and without sodium.

REFERENCES

1. A. Rockett, Thin Solid Films **480-481**, 2 (2005).
2. D. Rudmann, D. Bremaud, A. F. d. Cunha, G. Bilger, A. Strohm, M. Kaelin, H. Zogg, and A. N. Tiwari, Thin Solid Films **480-481**, 55 (2005).
3. C. Lei, C. M. Li, A. Rockett, and I. M. Robertson, J. Appl. Phys. **101**, 024909 (2007).
4. V. Lyahovitskaya, Y. Feldman, K. Gartsman, H. Cohen, C. Cytermann, and D. Cahen, J. Appl. Phys. **91**, 4205 (2002).
5. J. K. J. v. Duren, C. Leidholm, A. Pudov, M. R. Robinson, and Y. Roussilon, Mater. Res. Soc. Symp. Proc. 1012, 259 (2007).
6. W. N. Shafarman, R. Klenk, and B. E. McCandless, J. Appl. Phys. **79**, 7324 (1996).
7. P. T. Erslev, A. Halverson, W. Shafarman, and J. D. Cohen, Mater. Res. Soc. Symp. Proc. **1012**, 445 (2007).
8. J. T. Heath, J. D. Cohen, and W. N. Shafarman, J. Appl. Phys. **95**, 1000 (2004).
9. J. Lee, J. T. Heath, J. D. Cohen, and W. N. Shafarman, Mater. Res. Soc. Symp. Proc. **865,** 373 (2005).
10. S. Lany and A. Zunger, J. Appl. Phys. **100**, 113725 (2006).